Observation of Orbital Order in the Half-Filled 4*f* Gd Compound

H. Jang,[1] B. Y. Kang,[2] B. K. Cho,[2,*] M. Hashimoto,[1] D. Lu,[1] C. A. Burns,[1,3] C.-C. Kao,[4] and J.-S. Lee[1,†]
[1]*Stanford Synchrotron Radiation Lightsource, SLAC National Accelerator Laboratory, Menlo Park, California 94025, USA*
[2]*School of Materials Science and Engineering, Gwangju Institute of Science and Technology, Gwangju 61005, Korea*
[3]*Department of Physics, Western Michigan University, Kalamazoo, Michigan 49008, USA*
[4]*SLAC National Accelerator Laboratory, Menlo Park, California 94025, USA*
(Received 3 May 2016; published 18 November 2016)

Half-filled electron systems, even with the maximized spin angular moment, have been given little attention because of their zero-orbital angular moment according to Hund's rule. Nevertheless, there are several measurements that show evidence of a nonzero orbital moment as well as spin-orbit coupling. Here we report for the first time the orbital order in a half-filled $4f$-electron system GdB_4, using the resonant soft x-ray scattering at Gd $M_{4,5}$-edges. Furthermore, we discovered that the development of this orbital order is strongly coupled with the antiferromagnetic spin order. These results clearly demonstrate that even in half-filled electron systems the orbital angular moment can be an important parameter to describe material properties, and may provide significant opportunities for tailoring new correlated electron systems.

DOI: 10.1103/PhysRevLett.117.216404

According to Hund's rule [1], half-filled electron configurations, such as $3d^5$ and $4f^7$, lead to the zero-orbital angular momentum, $\boldsymbol{L} = 0$, while the spin angular momentum $\boldsymbol{S}$ is maximized. In this sense, no spin-orbit coupling is expected in half-filled electron systems. For this reason, therefore, an atomic element that has a half-filled electron configuration has been uninteresting for synthesis of strongly correlated electron systems. On the other hand, nowadays, the spin-orbit coupling interaction has been found to be an important parameter to design emergent materials such as topological insulators and superconductors, in addition to magnetic applications [2–7]. In particular, most exotic phenomena [2] in strongly correlated electron systems and, correspondingly, their complex phase diagrams [3,4] are attributed to an intercoupling between several degrees of freedom, including the spin-orbit coupling interaction [5–7]. To reinforce this interaction in material design, researchers have employed elements which have a large spin and/or orbital moment. In this context, half-filled systems have been given little attention even with the maximized spin moment, because of their zero-orbital moment.

Interestingly, in the last decade, many studies have demonstrated experimentally that the orbital angular momentum in half-filled systems does not follow Hund's rule [8–13]. For example, a nonzero d-orbital moment in Fe^{3+} (d^5 configuration) systems, e.g., $GaFeO_3$ and ϵ-Fe_2O_3 compounds, has been observed by soft x-ray magnetic circular dichroism measurements at the Fe L-edge [8,9]. In the Ca-doped $BiFeO_3$ compound, the anisotropically reconstructed Fe^{3+} d-orbital band was observed by resonant soft x-ray scattering [10]. Similarly, a considerable f-orbital moment contribution in the rare-earth metal Gd ($4f^7$ configuration) has been observed by using time-resolved x-ray experiments [11,12]. These experimental demonstrations imply that the orbital angular momentum is a non-negligible degree of freedom. Moreover, this implication makes a connection with previous findings [14,15] that observed a change in the g factor from the free electron value and a splitting of the Gd^{3+} ($4f^7$) Hund's rule ground-state manifold, revealing that the spin-orbit coupling effect, even in a half-filled system, is an important parameter. In this context, half-filled electron systems can be regarded as the strongly correlated electron systems. Several authors have considered the correlated effect theoretically [16,17]. Nevertheless, half-filled electron systems are still at an early stage of being accepted as an important issue in materials science. This is because no experimental demonstration of spin and orbital degree of freedom under the nonzero spin-orbit coupling has been performed in half-filled electron systems. Therefore, exploring static spin and orbital orders as well as their intercoupling behavior are critical to determine whether a half-filled system can be used to help design new materials.

To assess such a critical advance, we employ GdB_4 as a model system. GdB_4 has a primitive tetragonal structure ($P4/mbm$) with four formula units per lattice point as the basis [Fig. 1(a)] [18]. In the Gd metal case, the anisotropic $5d$ band is strongly coupled with the $4f^7$ band via intra-atomic exchange [25], leading to an f-orbital contribution in the half-filled Gd [11,12]. On the other hand, the ionic state becomes Gd^{3+} in Gd compounds like GdB_4, indicating a half-filled $4f^7$ configuration with an empty $5d$ band. However, through interatomic hybridization between the Gd $5d$ and B $2p$ states [26], the $5d$ orbital state undergoes a distortion, leading to the anisotropic $5d$ band [26,27]. As a consequence, the f-orbital contribution in GdB_4 is expected to be similar to Gd metal. Moreover, rare-earth

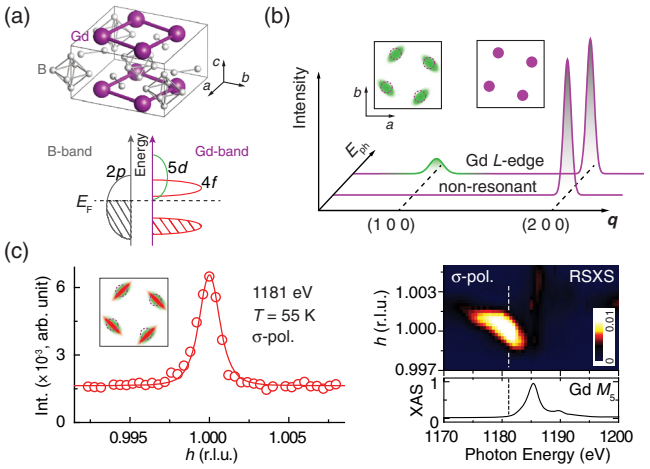

FIG. 1. (a) Crystal and schematic band structures of GdB_4. (b) Schematic diffraction patterns along $\boldsymbol{q} = (h \quad 0 \quad 0)$ at nonresonant or resonant Gd L-edge (d band). Insets represent Gd positions in the ab plane (right panel) and anisotropic $5d$ orbitals (left panel). (c) (left) The ATS $(1 \quad 0 \quad 0)$ reflection. The inset represents an overlay of the anisotropic $5d$ (green ellipse) and $4f$ (red ellipse) orbitals. (right) Top: the ATS resonant profile; bottom: the XAS spectrum of GdB_4.

tetraborides (RB_4) with $\boldsymbol{L} \neq 0$ rare-earth elements show various ordering phenomena [28–31], such as antiferromagnetic (AFM) order, quadrupolar order, and structural transitions, as well as their intercoupling effect. In this Letter, we employ a resonant soft x-ray scattering (RSXS) technique on GdB_4. Exploring the transition from the f-band through dipole transition ($3d \rightarrow 4f$) at the Gd $M_{4,5}$-edges, we directly address nonzeroed f-orbital behavior even with Gd^{3+} (i.e., a half-filled $4f^7$ configuration) and investigate its coupling with the AFM spin order above and below the Néel temperature, $T_N = 42$ K.

As a first step, the f-orbital behavior of GdB_4 was explored using RSXS at the Gd $M_{4,5}$-edges. All RSXS experiments were carried out at beam line 13–3 of the Stanford Synchrotron Radiation Lightsource. Four Gd atoms are located at the $4g$ symmetry points in the crystalline ab plane of a tetragonal unit cell and B atoms fill the space between Gd atoms [Fig. 1(a)]. Beyond the interatomic hybridization between the Gd $5d$-B $2p$ states [26], with the intra-atomic coupling the distorted $5d$ band would also hybridize with the Gd $4f$ band [Fig. 1(a)]. Therefore, these intraatomic- and interatomic mixings of the Gd $5d$ band lead to an anisotropic f-band tensor of the x-ray susceptibility. A forbidden reflection, namely an anisotropic tensor susceptibility (ATS) reflection [31,32], is allowed in resonant x-ray scattering (similar to Jahn-Teller assisted orbital behavior in manganites [4]). Figure 1(b) schematically shows the ATS reflection of the Gd $5d$ band at 55 K, revealing a forbidden reflection at $\boldsymbol{q}(H \quad K \quad L) = (2n+1 \quad 0 \quad 0)$ seen at the resonant Gd L-edge ($2p \rightarrow 5d$) [31], which originates from the distorted d-orbital band within the crystal structure [left inset in Fig. 1(b)]. Since a resonance at the Gd $M_{4,5}$-edges results from the $3d \rightarrow 4f$ dipole transition, the ATS reflection seen by RSXS indicates an anisotropic f band in the GdB_4 chemical environment. As we expected, the $4f$ band's ATS $(1 \quad 0 \quad 0)$ reflection is clearly observed by the RSXS measured in the paramagnetic state [Fig. 1(c)]. The ATS reflection shows resonant enhancement at the photon energy $(E_{ph}) \sim 1181$ eV. Note that the resonant energy position is slightly lower than the maximum seen in Gd x-ray absorption spectroscopy (XAS). The ATS resonance persists up to room temperature [18]. This indicates that the Gd f-orbital band is anisotropic; i.e., $\boldsymbol{L} \neq 0$, via the Gd $4f$-$5d$ hybridization, even in the half-filled configuration.

At $T > T_N$, where no long-range ordered spin contribution (i.e., AFM order) in GdB_4 [33] is expected, we found clear $4f$-orbital anisotropy due to Gd $4f$-$5d$ hybridization. To explore coupling between the anisotropic $4f$ orbital and the AFM phase, the RSXS measurements were performed below T_N. Figure 2(a) shows the AFM Gd spin configuration and the RSXS experimental geometry [18]. The scattering plane lies exactly in the crystalline ac plane. In the crystal's ab plane, a noncollinear arrangement of Gd spins [34] leads to AFM order, creating scattering intensity at the wave vector $\boldsymbol{q}(H \quad K \quad L) = (1 \quad 0 \quad 0)$, which is the same as the ATS reflection $\boldsymbol{q}$. With the scattering geometry shown in Fig. 2(a), therefore, the $(1 \quad 0 \quad 0)$ AFM therefore represents Gd spin components projected along the b axis. Further considering photon polarizations, with $\psi = 0°$ the $(1 \quad 0 \quad 0)$ AFM scattering intensity can only detect the AFM order through the π'-π channel, $\sim|-\cos\psi|^2_{\pi}$ [details in Eq. (S11) [18]]. In other words, it is impossible to detect any magnetic signal with an incident σ polarization at $\psi = 0°$. In this sense, with the incident π polarization, we could observe a clear AFM intensity at $T = 28$ K [Fig. 2(b)]. Interestingly, a clear resonant reflection is observed in the σ polarization [see the

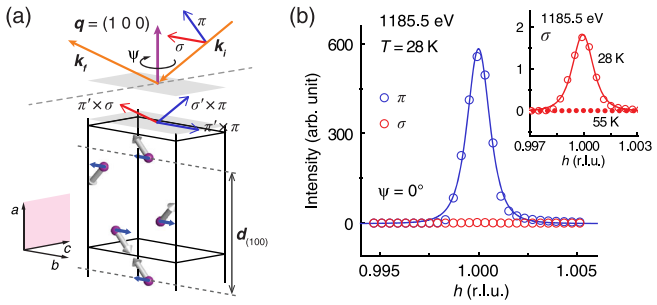

FIG. 2. (a) The RSXS experimental geometry ($\psi = 0°$) and its polarization configuration, and the Gd AFM spin structure. $\boldsymbol{k}_i$ ($\boldsymbol{k}_f$) denotes incident (scattered) photons. Blue arrows in the spin structure represent the projected Gd spins along the b axis. $\boldsymbol{d}_{(100)}$ indicates the real-space periodicity of the $(1 \quad 0 \quad 0)$ wave vector. (b) $(1 \quad 0 \quad 0)$ reflections below T_N ($T = 28$ K) in the π channel. The inset shows the σ channels.

inset of Fig. 2(b)]. Note that the observed intensity in the σ polarization is about two orders weaker than that in the π polarization. Hence, we infer that such an unexpected resonance in the σ channel must be associated with either the ATS reflection or something else (e.g., orbital order). Importantly, GdB_4 does not undergo any structure transition as a function of temperature [35] (see the Supplemental Material [18]), indicating a conservation of the crystal symmetry above and below T_N. For this reason, no significant temperature dependence of the ATS reflection is expected. As compared in the inset of Fig. 2(b), however, the σ-channel intensity below T_N is much stronger ($\sim \times 100$) than the pure ATS intensity above T_N. Thus, this σ-channel feature can be distinguished from the ATS reflection.

In order to investigate the origin of this σ-channel feature, the resonant energy profiles of $\boldsymbol{q} = (1 \quad 0 \quad 0)$ in both the σ and π channels were monitored [Fig. 3(a)]. Those two resonant profiles are not identical, showing a different intensity distribution as a function of E_{ph}. Note that the slight variation (the white dashed lines) of the $\boldsymbol{q}$ vector as a function of E_{ph} is proportional to a change in the real part of the atomic form factor [18,36]. In the π-channel case (i.e., the AFM reflection), the resonant maximum is at $E_{\mathrm{ph}} = 1188$ eV. Also, there are two relatively weak multiplets of Gd^{3+} at 1181 and 1184 eV. On the other hand, the resonant maximum in the σ channel (1184 eV) is 4 eV below the maximum for the magnetic order. This proves that the σ channel's feature is distinct from the magnetic order. It is worth noting that the small intensity spot in the σ channel that exists at 1188 eV might come from the imperfect incident x-ray polarization (98%). Moreover, the σ resonant profile is quite different from the ATS one shown in Fig. 1(d). In parallel, this energy-selective sensitivity is also supported by analysis of the Gd XAS, which consists of a combination of three terms due to the dipole selection rule $\Delta J = 0, \pm 1$ [18,37]. In particular, the quadrupole term is proportional to the absorption cross-section for $\Delta J = 0$, i.e., $F'(\Delta J = 0) + iF''(\Delta J = 0)$ [18,38,39]. As shown in the bottom of Fig. 3(b) the maximum resonance in the scattering profile in the σ channel is qualitatively represented by the $|F'(\Delta J = 0)|^2$ spectrum, revealing that the σ profile originates from the quadrupole moment. In this sense, we clearly exclude both the magnetic order and the pure ATS reflection as candidates for the origin of this σ-channel feature.

Another candidate, orbital order, is natural to consider. To check this possibility, the azimuthal angle dependences in both the π and the σ polarizations were performed. Similar to deriving the AFM intensity, we can first describe the orbital-scattering intensity in the incident σ polarization at $\psi = 0°$, $\sim|\cos\theta\cos\psi|^2_\sigma$ [details in Eq. (S15) [18]]. Accordingly, we infer that the signal in the incident σ polarization at $\psi = 0°$ is from the orbital. If $\psi \neq 0°$ (or $\neq 90°$), however, we must consider that the scattering intensities are from both the AFM and orbital ordering intensities because all components are nonzero. Therefore, we combined both orders and describe the total scattering intensities in the σ and π polarizations as follows [18]:

$$I_\sigma(\psi) = |-\mathcal{S}\cos\theta\sin\psi + \mathcal{O}\cos\theta\cos\psi|^2$$
$$I_\pi(\psi) = |\mathcal{S}\cos\theta\sin\psi + \mathcal{O}\cos\theta\cos\psi|^2 + |-\mathcal{S}\cos\psi|^2, \quad (1)$$

where $\mathcal{S}$ and $\mathcal{O}$ are, respectively, scattering factors which are proportional to the ordered spin and orbital moment. In this context, with a small variation from $\psi = 0°$, we can easily monitor a mixed feature containing both spin and orbital orders. For example [see Fig. 3(b)], it clearly shows the mixed feature (black circles) between the spin and orbital even with $\psi = 3.5°$. Using a linear combination of both the σ and π intensities at the $\psi = 0$ [i.e., $I_\sigma(0) \rightarrow$ orbital and $I_\pi(0) \rightarrow$ spin, and experimentally $\mathcal{S} \gg \mathcal{O}$], we produced the mixed feature [black solid line in Fig. 3(b)],

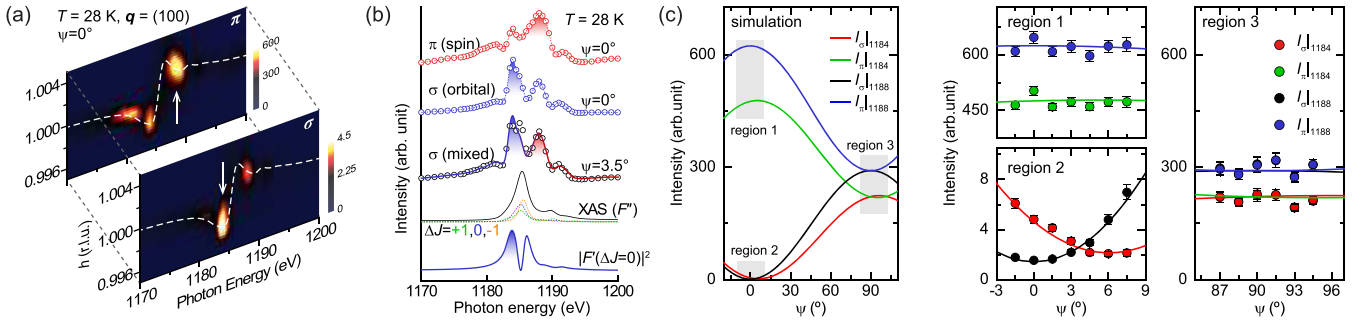

FIG. 3. (a) Two-dimensional maps of the $(1 \quad 0 \quad 0)$ resonant profiles in the σ and π channel. The arrows indicate the strongest resonant positions. The white dashed lines indicate slight variations of the wave vector due to the real part (F') of the atomic form factor. (b) Integrated resonant profiles in the π channel ($\psi = 0°$) and the σ channels ($\psi = 0°$ and 3.5°) as a function of the photon energy. At $\psi = 3.5°$, the black-solid line is the estimation. XAS spectrum is displayed with three dotted lines ($\Delta J = 0, \pm 1$) [18]. The bottom spectrum shows the squared atomic form factors with $\Delta J = 0$. (c) (left panel) Simulated azimuthal angle dependences with different photon energies and polarizations. (middle and right panel) Comparison between simulated (lines) and experimental (circles) results. The three regions are denoted as grey areas in the left panel.

which is well matched with the experimental azimuthal data.

Moreover, we expand the azimuthal angle study at the specifically tuned E_{ph}, because the orbital (1184 eV) and spin (1188 eV) resonances are energetically distinguishable. Figure 3(c) summarizes the simulated azimuthal angle dependences (left panel) of Eq. (1) depending on the photon energy and polarizations, as well as the comparison with experimental data (middle and right panels), resulting in good agreement. Note that details of parameters are in Ref. [18]. On the one hand, the overall spin's azimuthal dependences at the σ and the π channels are $\sim|\sin(\psi)|^2$ and $\sim|-\cos(\psi)|^2$, respectively. On the other hand, as shown in Fig. 3(c), the overall orbital response still looks like $\sim|\sin(\psi)|^2$ even with the σ channel at 1184 eV. This is because the spin-ordering signal is predominant even at the orbital resonant energy. However, the actual $I_\sigma|_{1184\ \mathrm{eV}}$ (i.e., orbital response) is nonzero at $\psi = 0$ [see the middle-bottom panel of Fig. 3(c)]. The minimum $I_\sigma|_{1184\ \mathrm{eV}}$ locates at $\psi \sim 6°$. According to Eq. (1), this shifted minimum indicates the existence of the nonzero $\mathcal{O}_{1184\ \mathrm{eV}}$, resulting in an interference effect between the AFM and orbital orders [18]. From these findings, we therefore conclude that the origin of the σ channel is mainly Gd $4f$-orbital order.

Considering the $4f$-orbital configurations in other RB_4 compounds [40,41], this orbital order might be quadrupolar order. In the other RB_4 compounds with $\boldsymbol{L} \neq 0$ rare-earth elements, it is known that the $4f$ quadrupolar order is closely correlated with the in-plane AFM magnetic structures through spin-orbit coupling [31]. For example, an antiferro-quadrupolar (AFQ) order at $\boldsymbol{q} = (1\ \ 0\ \ 0)$ in DyB_4 forms only when the in-plane noncollinear spin components of the AFM order develop [31]. At higher temperature, the AFM spin component is parallel to the out-of-plane direction, and no AFQ order appears. Similarly, we can associate the newly observed Gd $4f$-orbital order at $\boldsymbol{q} = (1\ \ 0\ \ 0)$ with the AFQ order if we find a similar relationship between the in-plane AFM order and the orbital order. Such a relationship was investigated by the temperature dependences of both the AFM order and the orbital order [Fig. 4(a)]. We found that an onset temperature of the orbital order coincides with T_N, indicating that the newly observed Gd $4f$-orbital order is the AFQ order.

While the AFM order shows the typical power-law behavior, however, the temperature behavior of the AFQ order is quite distinguishable from that of the AFM order. To understand the order parameter shapes, both the AFM and AFQ orders were fit using a power law $[1-(T/T_c)]^{2\beta}$. The AFM order is well described with T_c and 2β given by 41.8 ± 1 K and 0.78 ± 0.02, respectively. We note that the estimated β is very similar to the value in the three-dimensional Heisenberg magnet model [42], which is consistent with the noncollinear spin configuration in GdB_4 [34]. On the other hand, in the AFQ case, the 2β is estimated to be 0.97 ± 0.02, more than 20% slower than the

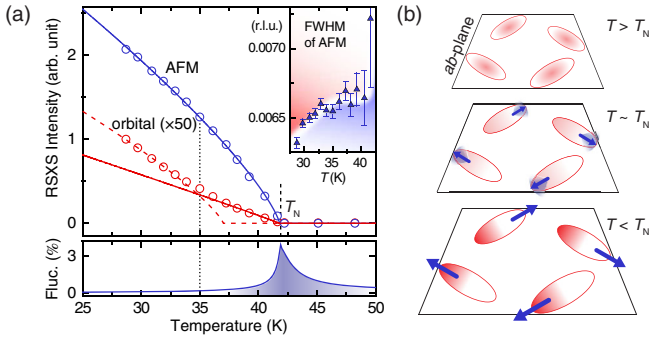

FIG. 4. (a) Temperature dependences of the integrated intensities of the AFM order (at 1188 eV, π) and orbital order (at 1184 eV, σ) with power-law fits and simulated spin fluctuation. The inset displays the FWHM (i.e., 1 divided by the correlation length) change in the AFM order, as a function of temperature. (b) Schematic picture of the evolutions of both spin (arrows) and orbital (ellipses) orders in the Gd $4f$ band as a function of temperature.

AFM order development. However, this 2β value does not fit below $T \sim 35$ K, due to the relatively faster growth of the AFQ intensity. The order parameter in the low-temperature region was fit by $2\beta = 0.79 \pm 0.02$, which is similar to the AFM order as well as the AFQ order in DyB_4 [31]. These fitting results indicate that the AFQ order in the temperature region $\sim 35\ \mathrm{K} < T < 42$ K is somewhat different from the AFQ order below 35 K. To understand this region, we simulated the Gd spin fluctuations using a Ginzburg-Landau free-energy model [18]. In the GdB_4 case, the simulation result is shown in the bottom panel of Fig. 4(a). Below T_N, the spin fluctuation is continuously decreasing. Interestingly, the vanishing point of the fluctuation occurs at $T \sim 35$ K, revealing that the slow development of the AFQ order is likely related with spin fluctuations. When the AFM order is fully developed, the AFQ order becomes reinforced. In other words, this AFQ order is induced by the AFM order through spin-orbit coupling. Furthermore, the AFM order below 35 K is affected by the reinforced AFQ order, resulting in the increased AFM correlation length [inset in Fig. 4(a)]. These implications are schematically summarized in Fig. 4(b). We note that the alignment of the orbital and magnetic orders also provides a possible reason for the AFM pattern found in this system, due to its spin-orbit coupling, and that the AFQ pattern in Fig. 4(b) used the same pattern as DyB_4 [31] because the in-plane AFM patterns in both GdB_4 [34] and DyB_4 [31] are identical.

In summary, we demonstrate for the first time the existence of orbital order in the half-filled $4f$-electron system, GdB_4, using resonant soft x-ray scattering. We also reveal that the orbital order is strongly coupled with the antiferromagnetic spin order. Considering these findings as well as the intrinsic advantage such as the maximized spin moment, the half-filled electron system may be appreciated as a new ingredient for materials design. The current Letter highlights a compelling new opportunity for tailoring

emergent functionality in strongly correlated electron systems.

We thank Warren E. Pickett, Ki Bong Lee, and Young S. Lee for valuable discussions and comments. All synchrotron studies were carried out at the Stanford Synchrotron Radiation Lightsource (SSRL), a Directorate of SLAC and an Office of Science User Facility operated for the U.S. Department of Energy (DOE) Office of Science by Stanford University. J.-S. L. acknowledges support by the Department of Energy, Office of Basic Energy Sciences, Materials Sciences and Engineering Division, under Contract No. DE-AC02-76SF00515. C. A. B. was supported by the U.S. Department of Energy, Office of Basic Energy Sciences, Division of Materials Sciences and Engineering, under Award No. DE-FG02-99ER45772. B. Y. K. and B. K. C were supported by National Research Foundation of Korea (NRF) grants funded by the Korean government (Ministry of Science, ICT and Future Planning, MSIP; Grants No. 2011-0028736 and No. 2013K000315).

*chobk@gist.ac.kr
†jslee@slac.stanford.edu

[1] C. Kittel, *Introduction to Solid State Physics*, 7th ed. (John Wiley and Sons, Inc., New York, 1996).
[2] L. A. Wray, S.-Y. Xu, Y. Xia, Y. S. Hor, D. Qian, A. V. Fedorov, H. Lin, A. Bansil, R. J. Cava, and M. Z. Hasan, Nat. Phys. **6**, 855 (2010).
[3] S.-W. Cheong and M. Mostovoy, Nat. Mater. **6**, 13 (2007).
[4] E. Dagotto and Y. Tokura, MRS Bull. **33**, 1037 (2008).
[5] A. D. Caviglia, M. Gabay, S. Gariglio, N. Reyren, C. Cancellieri, and J.-M. Triscone, Phys. Rev. Lett. **104**, 126803 (2010).
[6] V. Galitski and I. B. Spielman, Nature (London) **494**, 49 (2013).
[7] A. Manchon, H. C. Koo, J. Nitta, S. M. Frolov, and R. A. Duine, Nat. Mater. **14**, 871 (2015).
[8] J.-Y. Kim, T. Y. Koo, and J.-H. Park, Phys. Rev. Lett. **96**, 047205 (2006).
[9] Y.-C. Tseng, N. M. Souza-Neto, D. Haskel, M. Gich, C. Frontera, A. Roig, M. van Veenendaal, and J. Nogués, Phys. Rev. B **79**, 094404 (2009).
[10] H. Jang, G. Kerr, J. S. Lim, C.-H. Yang, C.-C. Kao, and J.-S. Lee, Sci. Rep. **5**, 12402 (2015).
[11] M. Wietstruk, A. Melnikov, C. Stamm, T. Kachel, N. Pontius, M. Sultan, C. Gahl, M. Weinelt, H. A. Dürr, and U. Bovensiepen, Phys. Rev. Lett. **106**, 127401 (2011).
[12] C. E. Graves *et al.*, Nat. Mater. **12**, 293 (2013).
[13] G. van der Laan, E. Arenholz, A. Schmehl, and D. G. Schlom, Phys. Rev. Lett. **100**, 067403 (2008).
[14] B. G. Wybourne, Phys. Rev. **148**, 317 (1966).
[15] H. A. Buckmaster and Y. H. Shing, Phys. Status Solidi A **12**, 325 (1972).
[16] R. Skomski, A. Kashyap, and A. Enders, J. Appl. Phys. **109**, 07E143 (2011).
[17] T. Hotta, J. Phys. Soc. Jpn. **84**, 114707 (2015).
[18] See Supplemental Material at http://link.aps.org/supplemental/10.1103/PhysRevLett.117.216404 for the experimental and simulation details and additional data, which includes Refs. [19–24].
[19] B. D. Cullity and S. R. Stock, *Elements of X-Ray Diffraction*, 3rd ed. (Prentice Hall, NJ, 2001), Chap. 4.
[20] J. P. Hannon, G. T. Trammell, M. Blume, and D. Gibbs, Phys. Rev. Lett. **61**, 1245 (1988).
[21] S. W. Lovesey and S. P. Collins, *Scattering and Absorption by Magnetic Materials* (Clarendon, Oxford, 1996), Chap. 5.
[22] H. Wadati *et al.*, J. Appl. Phys. **106**, 083705 (2009).
[23] E. Stavitski and F. M. F. de Groot, Micron **41**, 687 (2010).
[24] P. C. Hohenberg and A. P. Krekhov, Phys. Rep. **572**, 1 (2015).
[25] M. Colarieti-Tosti, S. I. Simak, R. Ahuja, L. Nordström, O. Eriksson, D. Åberg, S. Edvardsson, and M. S. S. Brooks, Phys. Rev. Lett. **91**, 157201 (2003).
[26] Z. P. Yin and W. E. Pickett, Phys. Rev. B **77**, 035135 (2008).
[27] S. Ji, C. Song, J. Koo, K.-B. Lee, Y. J. Park, J. Y. Kim, J.-H. Park, H. J. Shin, J. S. Rhyee, B. H. Oh, and B. K. Cho, Phys. Rev. Lett. **91**, 257205 (2003).
[28] D. Okuyama, T. Matsumura, H. Nakao, and Y. Murakami, J. Phys. Soc. Jpn. **74**, 2434 (2005).
[29] D. Okuyama, T. Matsumura, T. Mouri, N. Ishikawa, K. Ohoyama, H. Hiraka, H. Nakao, K. Iwasa, and Y. Murakami, J. Phys. Soc. Jpn. **77**, 044709 (2008).
[30] Z. Fisk, M. B. Maple, D. C. Johnston, and L. D. Woolf, Solid State Commun. **39**, 1189 (1981).
[31] S. Ji, C. Song, J. Koo, J. Park, Y. J. Park, K.-B. Lee, S. Lee, J.-G. Park, J. Y. Kim, B. K. Cho, K.-P. Hong, C.-H. Lee, and F. Iga, Phys. Rev. Lett. **99**, 076401 (2007).
[32] V. E. Dmitrienko, Acta Crystallogr. Sect. A **40**, 89 (1984).
[33] B. K. Cho, J.-S. Rhyee, J. Y. Kim, M. Emilia, and P. C. Canfield, J. Appl. Phys. **97**, 10A923 (2005).
[34] J. A. Blanco, P. J. Brown, A. Stunault, K. Katsumata, F. Iga, and S. Michimura, Phys. Rev. B **73**, 212411 (2006).
[35] J. Fernández-Rodríguez, J. A. Blanco, P. J. Brown, K. Katsumata, A. Kikkawa, F. Iga, and S. Michimura, Phys. Rev. B **72**, 052407 (2005).
[36] R. B. Leighton, *Principles of Modern Physics* (McGraw-Hill, New York, 1959), Chap. 12.
[37] J. B. Goedkoop, B. T. Thole, G. van der Laan, G. A. Sawatzky, F. M. F. de Groot, and J. C. Fuggle, Phys. Rev. B **37**, 2086 (1988).
[38] H. Ott, C. Schüßler-Langeheine, E. Schierle, A. Yu. Grigoriev, V. Leiner, H. Zabel, G. Kaindl, and E. Weschke, Phys. Rev. B **74**, 094412 (2006).
[39] T. Nagao and J. Igarashi, J. Phys. Soc. Jpn. **77**, 084710 (2008).
[40] T. Hotta, Rep. Prog. Phys. **69**, 2061 (2006).
[41] Y. Kuramoto, H. Kusunose, and A. Kiss, J. Phys. Soc. Jpn. **78**, 072001 (2009).
[42] J. C. Le Guillou and J. Zinn-Justin, Phys. Rev. Lett. **39**, 95 (1977).